TASK QUARTERLY 9 No 1, 103–114

SIMULATIONS OF FLOW PATTERNS IN SILOS WITH A CELLULAR AUTOMATON: PART 2

JAN KOZICKI AND JACEK TEJCHMAN

Civil Engineering Department,
Gdansk University of Technology,
Narutowicza 11/12, 80-952 Gdansk, Poland
tejchmk@pg.gda.pl

(Received 10 June 2004; revised manuscript received 16 August 2004)

Abstract: An improved cellular automaton has been used to calculate the kinematics of non-cohesive granular materials during confined flow in mass and funnel flow model silos. In this model, based on a gas model of hydrodynamics, collisions and dissipation of particles were taken into account during granular flow. The model allowed for investigations of dilatant zones in granular material during silo flow.

Keywords: cellular automaton, collision, density wave, granular flow, flow pattern, silo

1. Introduction

In the first paper on the cellular automaton [1], a simplified model was introduced to describe granular flow in silos with and without inserts. The granular flow of separate grains in silos was described as an upward propagation and diffusion of holes through a lattice of cells representing the granulate (grains moved downwards and voids moved upwards).

In this paper, an improved cellular automaton is used to determine flow patterns of non-cohesive granular bodies in model silos. In the model, based on a gas model of hydrodynamics, inelastic collisions and dissipation were taken into account [2–4]. The simulation results were compared with laboratory experiments performed with mass and funnel flow model silos [1]. In the mass flow silo, the entire material was in motion during discharge. In the funnel flow silo, movement was restricted to a channel within the stored material [5].

2. Description of the model

In a cellular automaton based on a lattice gas automaton [2, 4], some mechanical principles were taken into account. The model has enabled us to investigate propagating dilatant zones, which are an inherent characteristics of each discharge process in mass and funnel flow hoppers and parallel-converging bins during gravitational and controlled outflow of dense granular material composed of rough grains [6–13]. In this

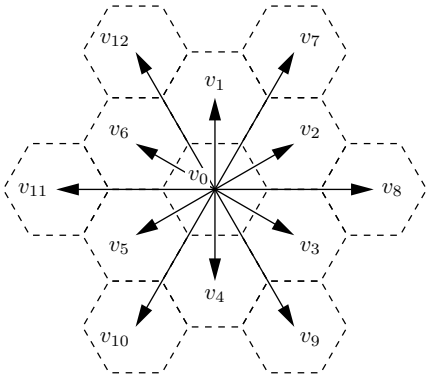

Figure 1. Vectors of particle velocities at each site

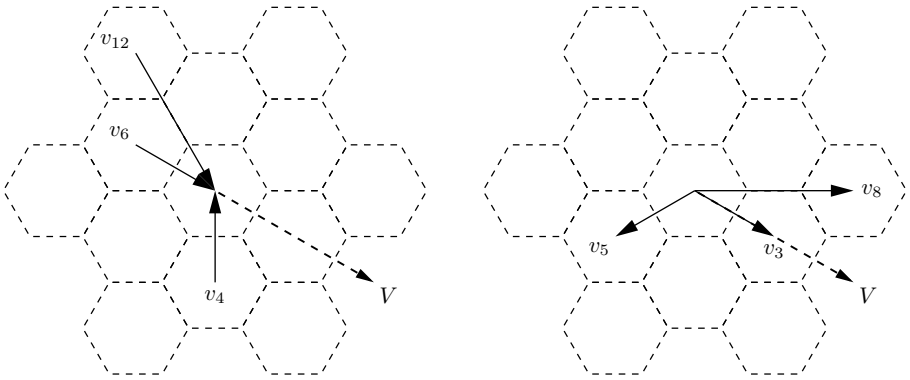

Figure 2. Velocity vectors of particles after collisions (V – resultant velocity)

mechanical model, each site of a hexagonal lattice could be occupied by one or more particles, a boundary wall or empty. The particles moved on the nearest-neighbor bonds (with unit velocity) and the second-nearest neighbors of the lattice (with unit velocity multiplied by the factor $\sqrt{3}$). Each particle at each site had 13 Boolean states which were related to velocity vectors v_i ($i = 0, 1, 2, \ldots, 12$, see Figure 1). The direction of motion of a particle, v, could be toward any of its 12 nearest neighbors ($i = 1, 2, \ldots, 12$) or the particle could be at rest ($v_0 = 0$). Thus, at the beginning of our calculations, the number of particles per site had a maximum value of 13 and a minimal value of 0. The time evolution consisted of one collision step and two propagation steps. In the collision step, both particles changed their velocities or remained at rest at the site by losing their total kinetic energy due to dissipation. In the first propagation step, particles (more than one) with no velocity were scattered randomly to the nearest empty sites with low numbers of particles. In the second propagation step, colliding particles (after changing their velocities) were transferred in the direction of their velocities to the nearest sites, where they collided again (see Figure 2). In general, collisions conserved mass and momentum. The simulations have shown that the calculation order of the lattice sites has no influence on the results. The following six parameters were assumed in the model: two collision parameters (p,q), two friction parameters (b,k) and two gravity parameters (g,h). All probabilistic parameters were in the range from 0 to 1.

The collision parameter p determined the number of particles, n, which remained at rest after a collision (due to energy dissipation). The $n$parameter was calculated from the following formula: $p^{(n+1)} < r < p^n$, where r is a random number. As some particles were stopped after collisions, other particles could leave the sites at with higher velocities, due to the conservation of momentum. When more than one particle was stopped and momentum could not be conserved, particles moved in random directions.

The q parameter described the loss of energy during each collision. The number of random particles, l, (which were not considered when calculating the resultant velocity) was obtained from the following formula: $q^{(l+1)} < r < q^l$. Due to the loss of energy, particles left sites with lower velocities. The total number of possible combinations for collisions was equal to $2^{12} = 4096$ and the number of possible velocity directions was 108. To accelerate the calculation process, an appropriate table of collisions was generated (Figure 3). If parameters p and q were equal to zero, the sum of velocity vectors outgoing from each site was equal to the sum of incoming velocity vectors (elastic collisions took place).

The friction parameter b described wall roughness. It was introduced in two different ways.

The first was based on the model proposed in [2]. If parameter b was other than zero (rough walls), particles bounced back from the wall in random directions. If $b = 0$ (smooth walls), the angle at which particles hit the wall was equal to the angle at which they were reflected.

In the second, particles hitting the wall were stopped there with a probability of b (the increase in wall roughness corresponded to the increase in parameter b). Afterwards, they were scattered randomly to the nearest empty sites with low contents of particles.

The friction parameter k described the internal interaction among particles. When parameter k was other than zero, certain migration directions could become more dominant (to induce movement in one specific direction). In our simulations, the horizontal direction was assumed to be dominant. Thus, the resulting velocity vector of outgoing particles was replaced by the sum of random velocity vectors in the directions v_2, v_3, v_5, v_6, v_8 and v_{11} (Figure 1) with a probability of k.

The gravity parameter g was taken into account during each collision by adding the vertical velocity, v_4, (Figure 2) to the resultant velocity vector of outgoing particles with a probability of g. Thus, the particles were accelerated downwards after each collision. At the same time, the gravity parameter h was introduced to improve the direction of the resultant velocity vector so that the direction would become parabolic for single particles (Figure 4). The particle remaining at rest at a given site (v_0) could move downwards to the v_0 state in the neighboring empty site with no velocity only in one of the chosen directions v_3, v_4, v_5, v_9 and v_{10} (Figure 1). If $h = 1$, particles without velocities moved downwards (density became more uniform). However, if $h = 0$, particles without velocities did not move.

The density of the granulate at the onset of flow dependent on parameters p, q, g and k was generated during silo filling when the outlet was closed. Having settled in the silo, the granular material reached certain density, which increased with increasing p and g and decreasing q and k.

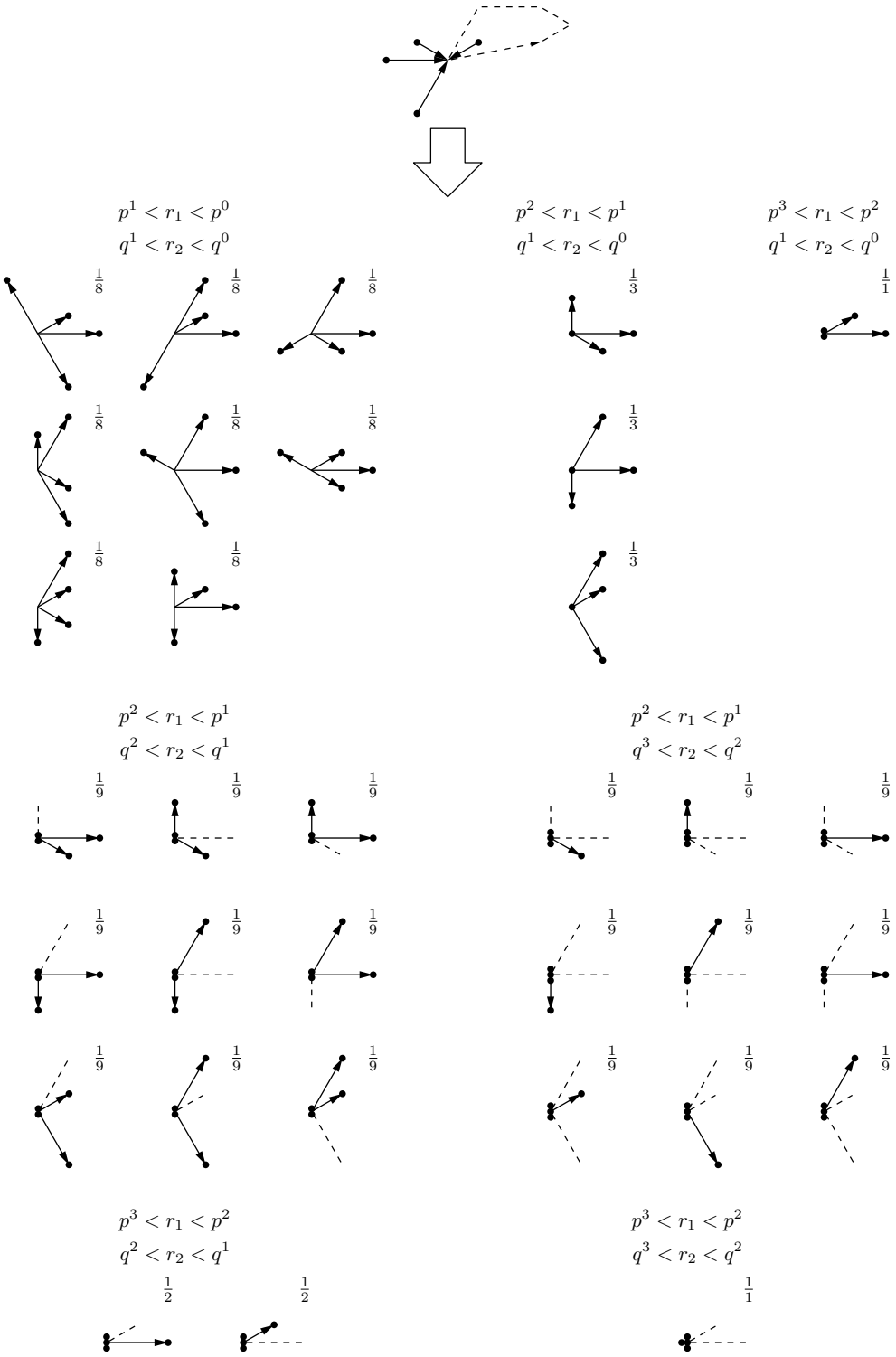

Figure 3. Examples of collision rules for 4 particles flowing to one site; the arrows represent the directions of moving particles, full dots stand for particles.

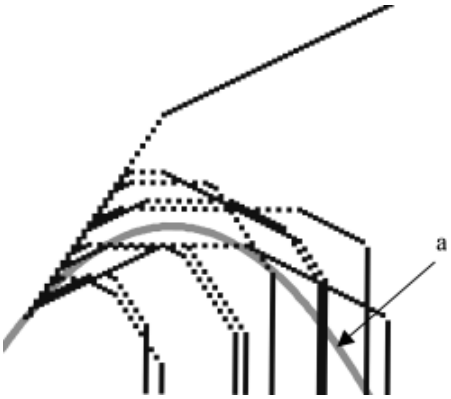

Figure 4. Example traces of single particles in the gravity field thrown from the same point in the direction of v_7 of Figure 2 (**a** – parabolic trajectory)

As mentioned above, the model is based on the approach proposed in [2, 4]. The following novelties were introduced: the number of possible vector directions was enhanced (13 instead of 7), density was not used as an additional parameter, gravitation was described by two parameters, rough walls were able to stop flowing particles, the method of describing collisions allowed to stop any number of particles, and a new parameter was introduced to describe the internal interaction among particles.

3. Simulation results

2D-results of simulations are shown in Figures 5–11 (mass flow silo) and Figures 12–18 (funnel flow silo). The shape and dimensions of the silos were similar to those of the laboratory tests described in [1, 14]. The number of cells was 35 000. The effect of parameters g, h, k, b, p and q is shown in Figures 6 and 13, Figures 7 and 14, Figures 8 and 15, Figures 9 and 16, Figures 10 and 17, and Figures 11 and 18, respectively for the mass and the funnel flow silos. The darker regions are associated with higher densities, while the lighter regions are associated with lower densities. In the calculations with parameter b, describing wall roughness, the second method was applied (the first, in contrast to results in a vertical pipe [6], did not affect the results in a silo). Initially, the values of parameters (Figures 5 and 12) were assumed to be random. Then, small and great parameter values were chosen for a comparison (Figures 6–11 and 13–18).

In all cases, regions of various density occur during granular flow. The shape of dilatant zones is similar for both flow types and is strongly influenced by the collision parameter p and the gravity parameter h. In the mass flow silo, it is also dependent upon the wall roughness parameter b (more particles are stopped at the wall region with increasing wall roughness). With the decreasing collision parameter p, the height of dilatant zones increases significantly (the material behaves more like gas). If the gravity parameter h is great, the dilatant zones become narrower and more concentrated in the middle region of the silo due to more empty sites appearing in the middle of the silo than in the region close to its walls. For smaller wall roughness parameters b, the dilatant zones are more horizontal (in the mass flow silo) since

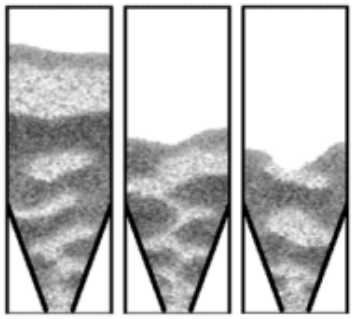

Figure 5. Flow pattern in a mass flow silo: $p=0.2$, $q=0.2$, $b=0.05$, $k=0.05$, $g=0.2$, $h=0.05$

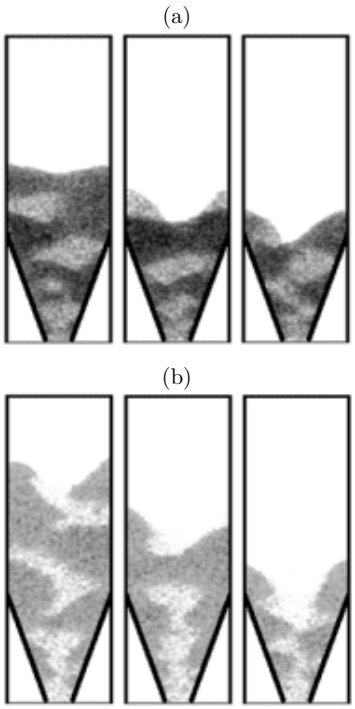

Figure 6. Flow pattern in a mass flow silo: (a) $p=0.2$, $q=0.2$, $b=0.05$, $k=0.05$, $g=0.95$, $h=0.05$; (b) $p=0.2$, $q=0.2$, $b=0.05$, $k=0.05$, $g=0.05$, $h=0.05$

the presence of walls disturbs less flow. The outflow rate obviously increases with the increasing gravity parameter g. With an increase of the gravity parameter g, the effect of other factors becomes insignificant. The inclination of the upper free surface of the material decreases with decreasing parameters p, q and h (the material then behaves more like gas). The non-uniformity of the material's density increases with increasing parameter g and decreasing parameters h, k, p and q.

Although the calculated flow patterns in silos are in satisfactory agreement with the experimental ones [1] (especially for the mass flow silo), the calculated shapes of the propagating dilatant zones in the flowing material differ from the experimental ones due to pure shearing of the granular material having been neglected. In the experiment with a mass flow silo [11, 12], a symmetrical pair of curvilinear dilatant

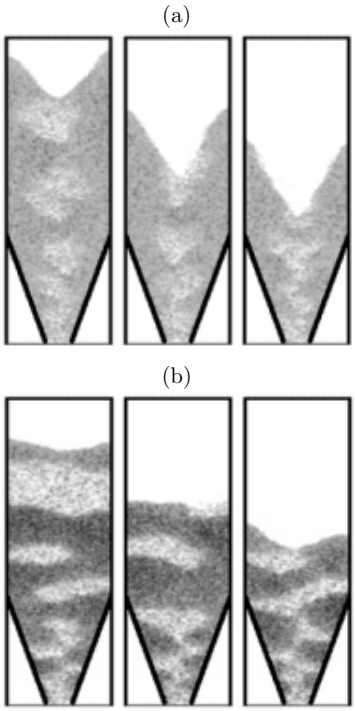

Figure 7. Flow pattern in a mass flow silo: (a) $p=0.2$, $q=0.2$, $b=0.05$, $k=0.05$, $g=0.2$, $h=0.8$; (b) $p=0.2$, $q=0.2$, $b=0.05$, $k=0.05$, $g=0.2$, $h=0.0$

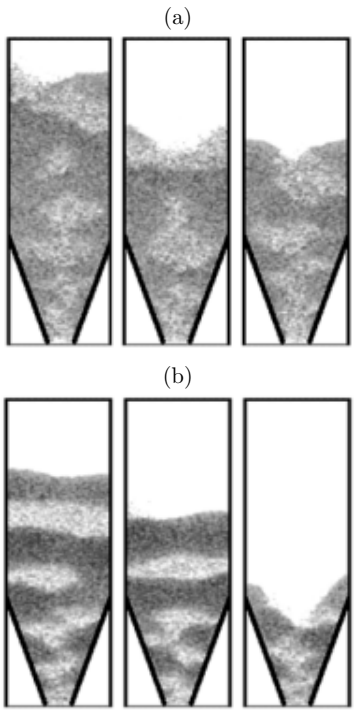

Figure 8. Flow pattern in a mass flow silo: (a) $p=0.2$, $q=0.2$, $b=0.05$, $k=0.8$, $g=0.2$, $h=0.05$; (b) $p=0.2$, $q=0.2$, $b=0.05$, $k=0.0$, $g=0.2$, $h=0.05$

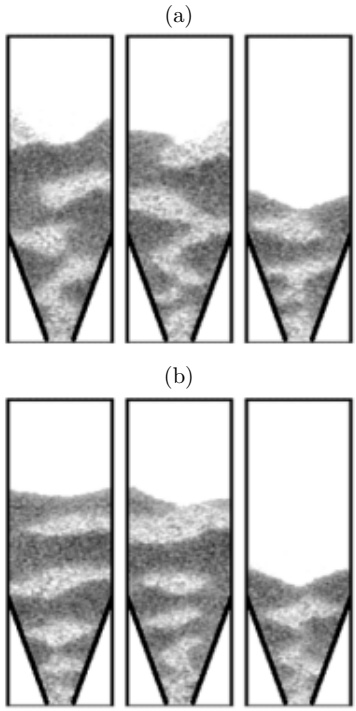

Figure 9. Flow pattern in a mass flow silo: (a) $p=0.2$, $q=0.2$, $b=0.8$, $k=0.05$, $g=0.2$, $h=0.05$; (b) $p=0.2$, $q=0.2$, $b=0.0$, $k=0.05$, $g=0.2$, $h=0.05$

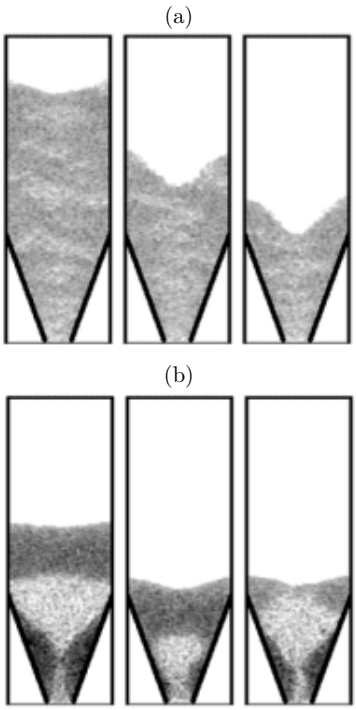

Figure 10. Flow pattern in a mass flow silo: (a) $p=0.8$, $q=0.2$, $b=0.05$, $k=0.05$, $g=0.2$, $h=0.05$; (b) $p=0.0$, $q=0.2$, $b=0.05$, $k=0.05$, $g=0.2$, $h=0.05$

(a)

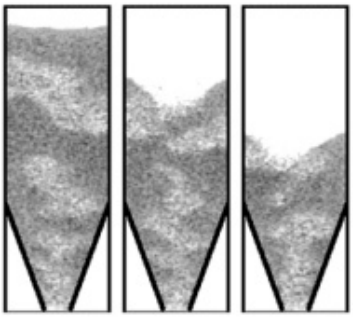

(b)

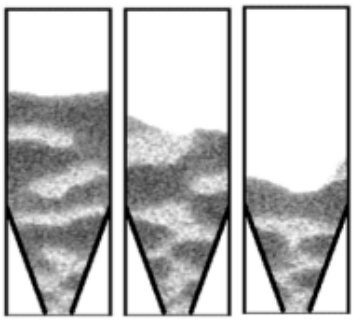

Figure 11. Flow pattern in a mass flow silo: (a) $p=0.2$, $q=0.8$, $b=0.05$, $k=0.05$, $g=0.2$, $h=0.05$; (b) $p=0.2$, $q=0.0$, $b=0.05$, $k=0.05$, $g=0.2$, $h=0.05$

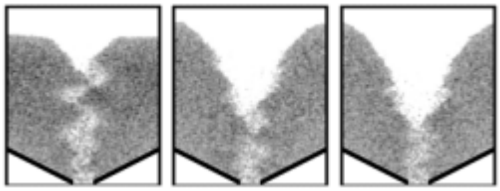

Figure 12. Flow pattern in a funnel flow silo: $p=0.2$, $q=0.2$, $b=0.05$, $k=0.05$, $g=0.2$, $h=0.05$

(a)

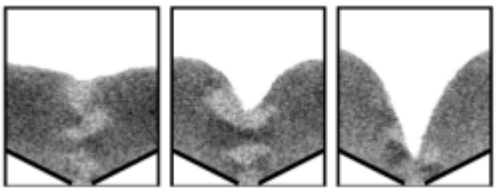

(b)

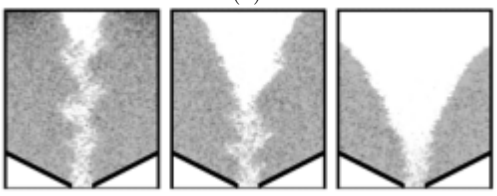

Figure 13. Flow pattern in a funnel flow silo: (a) $p=0.2$, $q=0.2$, $b=0.05$, $k=0.05$, $g=0.95$, $h=0.05$; (b) $p=0.2$, $q=0.2$, $b=0.05$, $k=0.05$, $g=0.05$, $h=0.05$

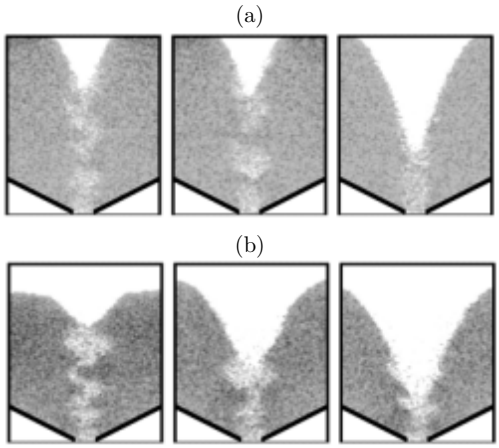

Figure 14. Flow pattern in a funnel flow silo: (a) $p=0.2$, $q=0.2$, $b=0.05$, $k=0.05$, $g=0.2$, $h=0.8$; (b) $p=0.2$, $q=0.2$, $b=0.05$, $k=0.05$, $g=0.2$, $h=0.0$

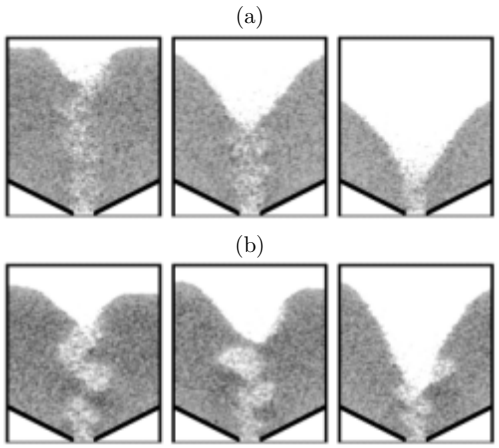

Figure 15. Flow pattern in a funnel flow silo: (a) $p=0.2$, $q=0.2$, $b=0.05$, $k=0.8$, $g=0.2$, $h=0.05$; (b) $p=0.2$, $q=0.2$, $b=0.05$, $k=0.0$, $g=0.2$, $h=0.05$

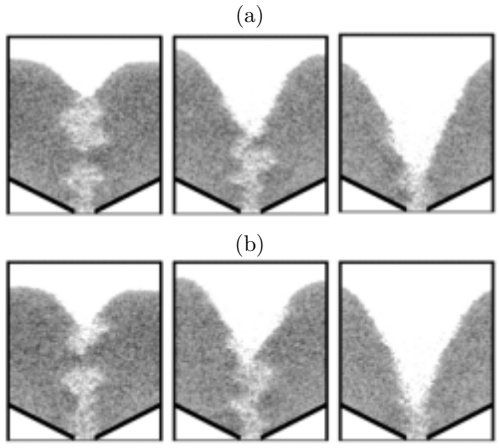

Figure 16. Flow pattern in a funnel flow silo: (a) $p=0.2$, $q=0.2$, $b=0.8$, $k=0.05$, $g=0.2$, $h=0.05$; (b) $p=0.2$, $q=0.2$, $b=0.0$, $k=0.05$, $g=0.2$, $h=0.05$

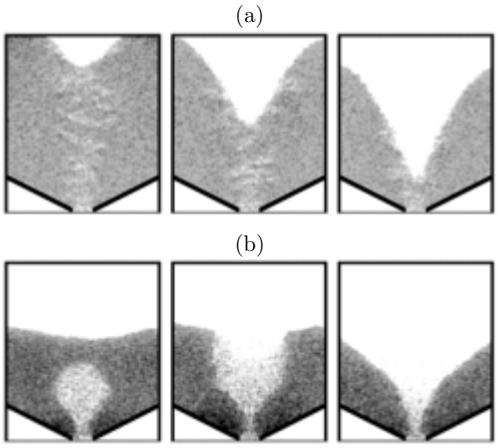

Figure 17. Flow pattern in a funnel flow silo: (a) $p=0.8$, $q=0.2$, $b=0.05$, $k=0.05$, $g=0.2$, $h=0.05$; (b) $p=0.0$, $q=0.2$, $b=0.05$, $k=0.05$, $g=0.2$, $h=0.05$

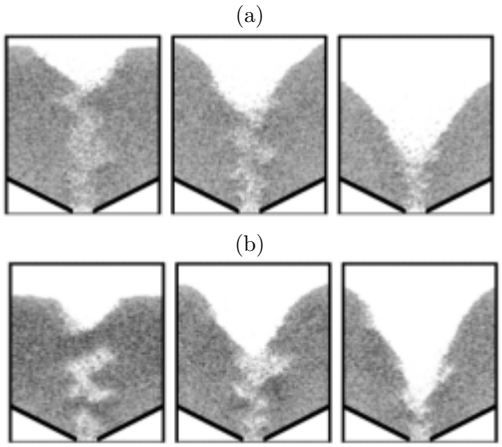

Figure 18. Flow pattern in a funnel flow silo: (a) $p=0.2$, $q=0.8$, $b=0.05$, $k=0.05$, $g=0.2$, $h=0.05$, (b) $p=0.2$, $q=0.0$, $b=0.05$, $k=0.05$, $g=0.2$, $h=0.05$

rupture zones was created in the neighborhood of the outlet. The zones propagated upwards, crossed each other around the symmetry of the silo, reached the walls and were subsequently reflected from them. This process was repeated until the zones reached the free boundary in the converging hopper or the transition zone in the parallel-converging silo. In the funnel flow silo [6, 7], the curvilinear dilatant zones in the material core were symmetric about a vertical mid-line. Some of them crossed each other.

4. Conclusions

Although cellular automata are purely kinematic models and simplify the behavior of granular materials, they can capture realistically flow patterns of granulates in silos on the basis of back analysis of laboratory experiments.

The advanced cellular automaton has been able to describe the propagation of dilatant zones in granular material during silo flow. Their shape was affected by

gravity, collision and friction parameters. However, it was different than that obtained in experiments.

References

[1] Kozicki J and Tejchman J 2005 *TASK Quart.* **9** (1) 81
[2] Peng G and Herrmann H J 1994 *Phys. Rev.* **49** (3) 1796
[3] Deserable D, Masson S and Martinez J 2001 *Powders and Grains* (Kishino, Ed.), Swets and Zeitlinger, Lisse, pp. 421–424
[4] Alonso J J and Herrmann H J 1996 *Phys. Rev. Lett.* **76** (26) 4911
[5] Safarian S S and Harris E C 1985 *Design Construction of Silos and Bunkers*, Von Nostrand Reinhold Company
[6] Baxter G W, Behringer R P, Fagert T and Johnson G A 1990 *Pattern Formation and Time-dependence in Flowing Sand. Two Phase Flows and Waves* (Joseph D D and Schaeffer D G, Eds.), Springer Verlag, New York, pp. 1–29
[7] Baxter G W and R P Behringer 1991 *Physica* **D 51** 465
[8] Cutress J and Pulfer R F 1967 *Powder Technology* **1** 212
[9] Bransby P L, Blair-Fish P M and James R G 1973 *Powder Technology* **8** 197
[10] Drescher A, Cousens T W and Bransby P L 1978 *Geotechnique* **28** (1) 27
[11] Michalowski R L 1984 *Powder Technology* **39** 29
[12] Michalowski R L 1990 *Geotechnique* **40** (3) 389
[13] Tejchman J 1997 *Publication Series of the Institute for Rock and Soil Mechanics, Karlsruhe University* **140** 1
[14] Kozicki J and Tejchman J 2001 *Int. J. Storing, Handling and Processing Powder (Powder Handling and Processing)* **13** (3) 267